

## Study on the Electrochemical Corrosion and Scale Growth of Ductile Iron in Water Distribution System

Hao Guo<sup>1,\*</sup>, Yimei Tian<sup>1</sup>, Hailiang Shen<sup>2</sup>, Xingfei Liu<sup>1</sup>, Ying Chen<sup>1</sup>

<sup>1</sup> School of Environmental Science and Engineering, Tianjin University, Tianjin 300072, China.

<sup>2</sup> GHD, 651 Colby Drive, Waterloo, ON, Canada, N2V 1C2.

\*E-mail: [tjuguohao@163.com](mailto:tjuguohao@163.com)

Received: 8 April 2016 / Accepted: 22 May 2016 / Published: 7 July 2016

---

A simulated water distribution system (WDS) combining specialized coupon test units and an electrochemical measurement cell is designed to provide an actual pipe corrosion environment. Coupon test is used to obtain the scale morphology and corrosion rate (CS), and provide scale samples for physicochemical characteristic analysis. Electrochemical impedance spectroscopy (EIS) is conducted simultaneously to display the scale structure change. Three corrosion stages are observed during a 32-day circulation. In initial stage (before day 4), the thin double-layer scales fast form inducing a sharp decline of CS (0.9455~0.1492 mm/a). In developmental stage (day 4~16), the loose scales grow uniformly and the CS decreases slowly (0.1492~0.0936 mm/a). In stable stage (after day 16), the protective scales with a compact outside layer finally form, and the CS maintains at a low value around 0.0900 mm/a. EIS fitting results showed that the stable scales consisted of a compact outside layer and a porous inside layer. In the stable stage, the increasing content of goethite and calcite slows the rate of dissolved oxygen diffusing through the scales, resulting in mass diffusion turning to be the rate-determining step of corrosion. Finally the mechanism of scale growth and localized tubercle formation is proposed.

---

**Keywords:** corrosion scales; EIS; XRD; ductile Iron; water distribution system

### 1. INTRODUCTION

Ductile iron (DI) pipes have been widely used in water distribution system (WDS) in North America since the late 1950s [1], and are the predominant metal pipes due to their high strength and resistance to corrosion. Their widely usage in China started in 1980s, and DI pipes are largely adopted for replacing cast iron pipes in recent WDS reconstruct engineering. In general, DI pipes are protected by cement mortar linings or other coatings from the direct contact with water. But due to external and

internal loads such as traffic loading, frost loads, operational pressure, and third party interference, the integrity of linings is compromised and tiny cracks appear randomly. Inadequate installation and manufacturing defects make it very common in China. Then DI is corroded by the delivered water penetrated through the cracks. The growth of corrosion scales can in turn expand the cracks and lead to detachment of linings. Thus the bare inner wall becomes the most vulnerable area occurring leakage and burst. As the interface of water and inner wall, the scales plays an important role in further corrosion. So research on its growth and characteristics is of great significance for DI pipes corrosion control and residual service life prediction.

Iron corrosion scales directly obtained from old pipes [2-6] have been widely studied and the research focused on its static characteristics such as morphology, physical structure and chemical composition. Sarin [7] proposed a conceptual model to describe the formation and growth of iron scales, but the model was only a framework and the detailed process needed further experimental verification. Immersion tests using iron coupons or electrodes were commonly conducted to gain better insight into the scale transformation. Each of them has their advantages in scale study. Iron coupons can generate corrosion scales for composition analysis [8-10] and provide reliable corrosion rate by weighting mass loss [11]. While iron electrodes are mainly used for non-destructive and real-time electrochemical measurement. Hereinto, electrochemical impedance spectroscopy (EIS) is an effective tool to reveal the structure of corrosion scales [12-15]. However, these tests were usually implemented in small-scale reactors (SRs). Thus the corrosion environment (water hydraulic and quality conditions) is very different from the actual WDS. Firstly, water hydraulic condition of WDS is hard to simulate in SRs. Although annular reactors [9] and rotating disk/cylinder electrodes (RDEs/RCEs) [16, 17] can provide laminar and turbulent flow status at the interface of iron and water, the centrifugal force damages the growth of scales and they cannot provide an actual growing condition liking the pipe internal wall. Secondly, the water quality of SRs is affected by the dissolved corrosion products and cannot remain unchanged. Whether SRs are sealed or inserted in a circulating system [17], the total volume of water in the experimental system is usually limited. After a long time of immersion or circulation, the water quality changes and deviates from the initial condition, and can adversely damage the further growth of scales.

Compared with SRs, pilot pipe distribution systems are more favorable for simulating actual WDS corrosion environment. But in these experiments [18-20], only the composition variation of scales were studied through iron coupons and pipe sections. Because the coupons or pipe sections need to be taken out of the system at fixed period for detection and weighing, so the continuous variation of scales is hard to be observed. In addition, the structure transformation of scales cannot be monitored without iron electrodes being plugged into the pilot system. Therefore integrating iron coupons and electrodes simultaneously into a pilot circulating system is a promising approach to study the growth and characteristics of corrosion scales. But to date most investigators have merely compared the results of coupons test and electrochemical measurements [11, 17] without integrating them into a new test system.

This paper designs a simulated WDS combining coupon test units and an electrochemical measurement cell. A water renewal system is equipped to update water quality during water circulation, so the simulated WDS can provide actual pipe corrosion environment to research the

electrochemical corrosion and scale growth of DI pipes. The detailed working principle of the system is shown in Section 2.1. Iron coupons are taken out of the system at fixed period for corrosion scales sampling and corrosion loss weighting. Simultaneously, electrochemical measurement is conducted in the electrochemical measurement cell to monitor the structure transformation of the scales. The morphology and corrosion rate of DI are obtained by coupon tests. The growth and transformation of the scales is examined by analysing EIS data. The elemental and crystalline composition of the corrosion scales is detected by scanning electron microscopy (SEM), energy dispersive spectroscopy (EDS), and X-ray diffraction (XRD). Finally, the mechanism of scale growth and related corrosion reactions are proposed.

## 2. MATERIAL AND METHODS

### 2.1 Simulated WDS

Figure 1 shows the schematic of the simulated WDS. This system includes four components: (I) water-quality renewal system, (II) piping system, (III) coupon test units, and (IV) an electrochemical measurement cell. Coupon test units and electrochemical measurement cell are connected in series. To provide uniform hydraulic condition, both of them have the same cross-section shape (round) and area ( $19.63 \text{ cm}^2$ ). The number of the coupon test units is determined by the sampling frequency.

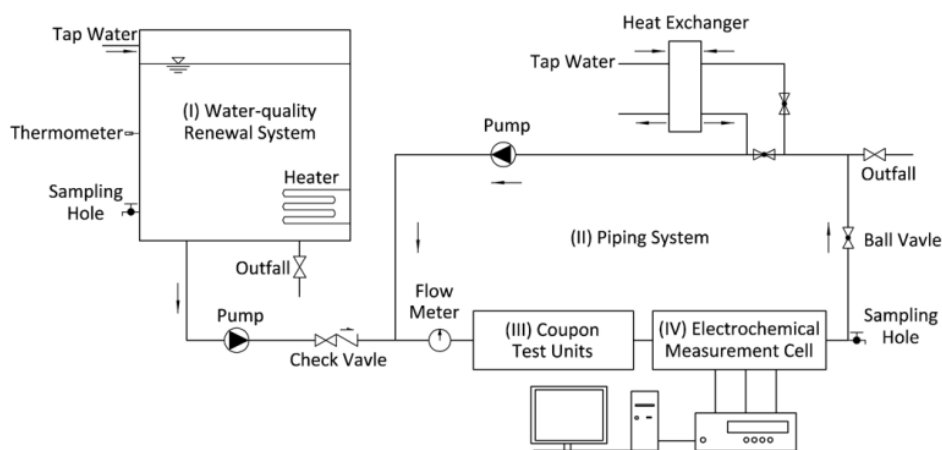


**Figure 1.** Schematic of the simulated WDS.

The water-quality renewal system includes a 500-litre polyethylene tank filled with tap water from the WDS of Tianjin, China. Water is pumped from the tank into the piping system. The circulating water can be discharged through the outfall and fresh water from the water-quality renewal system can be simultaneously added to the piping system. This simulated system can circulate water while updating water quality, which provides a corrosion environment close to the hydraulic and water-quality conditions of the actual WDS.

Figure 2 shows the schematic of the coupon test unit, which is comprised of a polymethyl methacrylate (PMMA) cylinder and a polytetrafluoroethylene (PTFE) plug. Test coupons (i) are fixed onto the PMMA baffle (ii) with a nylon screw and nut (iii). The inlet (iv) and outlet (v) made of PTFE enable the device to simulate the flushing condition of a pipe wall. A maximum of five coupons can be affixed to the baffle. Four of the five coupons are used for weighing corrosion loss and the remaining one is used for a physicochemical analysis of the corrosion scales.

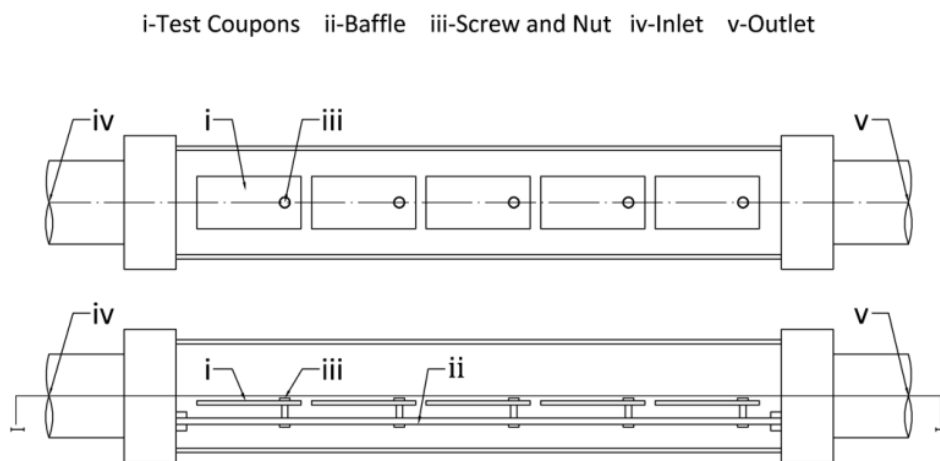


Figure 2. Schematic of coupon test unit.

A-Working Electrode B-Reference Electrode  
C-Counter Electrode D-Inlet E-Outlet F-Thermometer

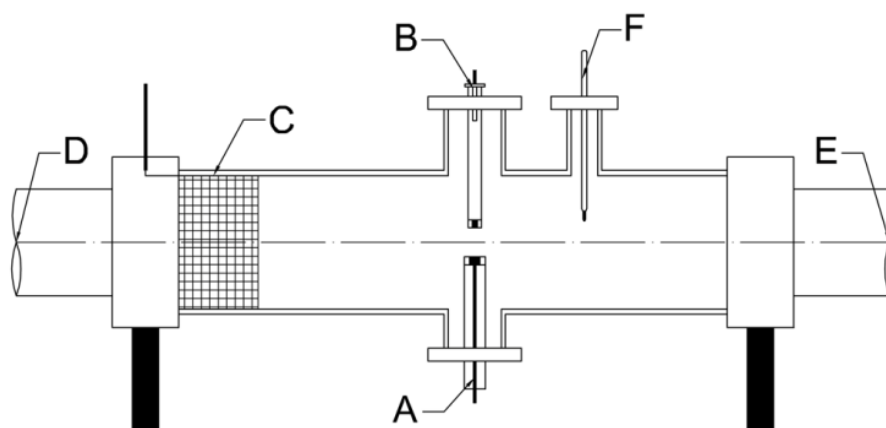


Figure 3. Schematic of electrochemical measurement cell.

Figure 3 shows the schematic of the electrochemical measurement cell. The cell consists of an annealed glass cylinder and a PTFE plug. In this cell, the working electrode (A) is vertically inserted into the cell, making its surface parallel to the water flow. Thus it can simulate the flushing condition

of the interior pipe wall. The reference electrode (B) - Saturated Calomel Electrode (SCE), is inserted into the glass salt bridge filled with saturated potassium sulfate solution. A large swatch of platinum mesh serves as the counter electrode (C).

### 2.2 Ductile iron coupon and tap water

A standard DI coupon (dimension 25×5×2 mm) is used in the coupon test unit. The working electrode used in the electrochemical measurement cell is made from a standard DI coupon with a surface area of 0.785 cm<sup>2</sup>. The composition of the DI coupon (provided by the manufacturer) is shown in Table 1.

**Table 1.** Composition of the test DI (wt %).

C	Si	Mn	P	S	Mg	Re	Fe
3.60	2.60	0.45	0.06	0.02	0.04	0.03	balanced

The coupons and electrode are abraded with silicon carbide paper, rinsed with distilled water, degreased with ethanol and acetone and subsequently dried in a vacuum desiccator at room temperature. Tap water taken directly from the City's WDS is used as the corrosion medium. Each water quality parameter is measured daily during the period of the experiment. The average values are listed in Table 2.

**Table 2.** Average parameter values of tap water.

pH	DO [mg·L <sup>-1</sup> ]	Total Hardness [mg·L <sup>-1</sup> as CaCO <sub>3</sub> ]	Total Alkalinity [mg·L <sup>-1</sup> as CaCO <sub>3</sub> ]	Cl- [mg·L <sup>-1</sup> ]	SO <sub>4</sub> <sup>2-</sup> [mg·L <sup>-1</sup> ]	Total Residual Chlorine [mg·L <sup>-1</sup> ]	Conductivity [μs·cm <sup>-1</sup> ]	TDS [ppm]
7.13	6.27	237.16	112.11	48.96	105.85	0.23	550	190

### 2.3 Procedure for coupon test

Considering the corrosion rate and scales change rapidly during the first few days and are relatively stable afterwards, the coupon test units were sampled on days 0.5, 1, 2, 4, 8, 12, 16, 20, 24, 28 and 32, respectively. Prior to the test, the dried DI coupons were weighed using an analytical balance with an accuracy of 10<sup>-4</sup> g; the weights were denoted as the original weight. After the immersion testing, DI coupons were firstly photographed with a high-definition digital camera (Canon digital single-lens reflex camera, EOS 700D) to obtain the corrosion morphologies. The corrosion products were removed with a hairbrush and the corroded coupons were rinsed with distilled water, a pickling solution, an alkaline solution, and ethanol; they were then dried in a desiccator for 24 hours and reweighed to obtain the final weight.

#### 2.4 Procedure for electrochemical measurement

When coupon test units were taken out from the simulated WDS, EIS was conducted in the electrochemical measurement cell to obtain the structure characteristics of the corrosion scale. Before each EIS measurement, the steady-state open circuit potential (OCP) was firstly recorded. Then EIS was performed on the steady-state OCP driven at an applied-amplitude alternating current (AC) signal of 10 mV and a frequency ranging from 100 kHz to 10 mHz. Zview 2.0 was used to collect the EIS data and ZsimpWin 3.10 was used to fit the parameters.

#### 2.5 Procedure for scales physicochemical characteristic analysis

The corrosion scales on corroded coupons were mechanically stripped off the corroded coupon surface and stored in a vacuum desiccator to avoid oxidation in the atmosphere. The larger fragments of dried corrosion scales were used to prepare SEM/EDS samples to examine surface integrity, and the remaining scales were ground into powder for the XRD analysis. A field-emission scanning electron microscope (Nanosem 430) was used to examine the microscopic surface morphologies and chemical composition of the corrosion scales. XRD (D/MAX-2500, with  $2\theta$  ranged from  $10^\circ$  to  $90^\circ$ ) was employed to identify the crystalline phase of the corrosion scales on the corroded coupon.

### 3. RESULTS AND DISCUSSION

To guarantee the accuracy and reproducibility of the results, two sets of parallel experiments have been conducted. Both of the results are consistent well with each other, so one of the two results is discussed in the following sections.

#### 3.1 Coupon test analysis

##### 3.1.1 Scale morphology

Figure 4 shows the typical photographs taken from the DI coupons showing the growth of corrosion scales of DI in simulated WDS. With the increasing of circulation time, three scale states can be seen: (1) a thin and incomplete scale layer (12h~2d); the thin film of green corrosion products (12h) quickly became reddish (1d) and then formed an incomplete layer on the coupon surface (2d). (2) a smooth and loose scale layer (4d~16d); although some defects randomly appeared on the surface of scale caused by flowing water in this stage, the scale surface basically maintained flat and general corrosion is the predominant corrosion type. (3) a rough and compact scale layer (20d~32d); localized corrosion occurred and the even scale surface gradually became irregular and inhomogeneous.

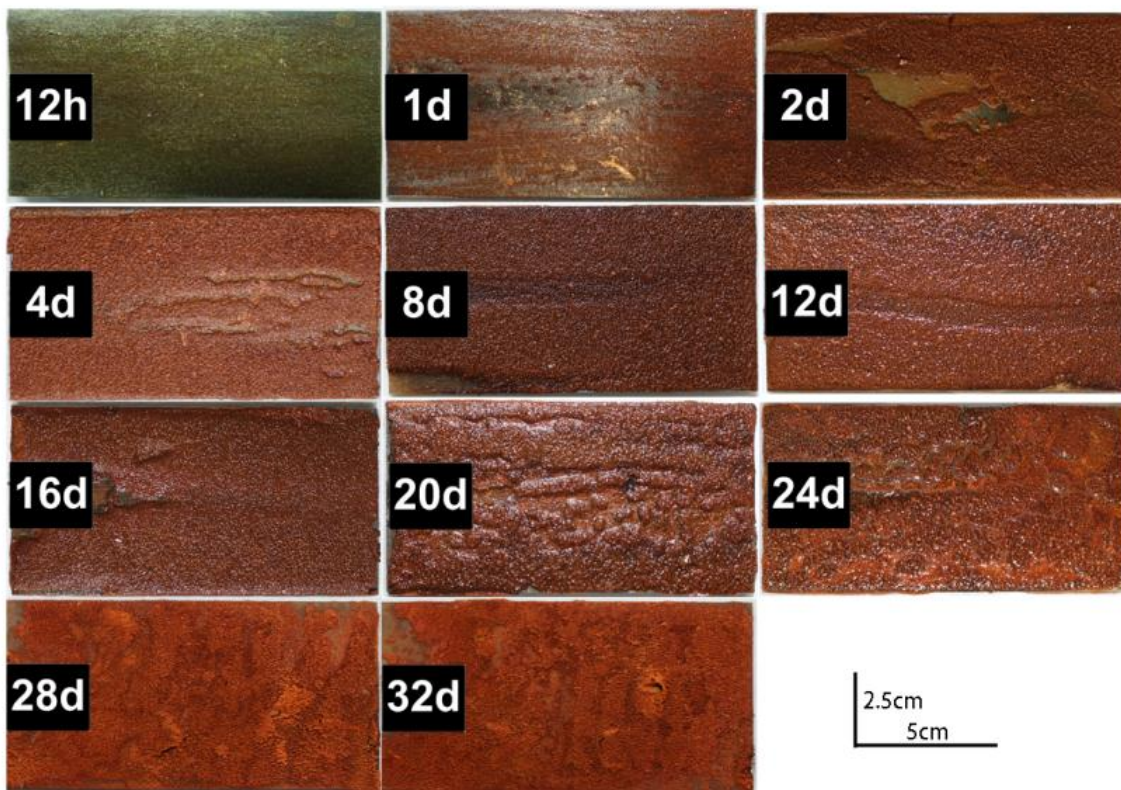


**Figure 4.** Morphologies of DI corrosion scales in simulated WDS.

On the whole, the corrosion scale firstly experiences a four-day fast growth to achieve a basic coverage, and then enters slowly uniform growth between the fourth day and sixteenth day. After the sixteenth day, the scale surface turns to be rough and compact, finally resulting in the formation of tubercles.

### 3.1.2 Corrosion rate

Figure 5 shows the corrosion loss and rate of DI calculated from the corroded coupons. Corrosion rate for specified period  $v_{WLM,i}$  is calculated with Equation (1)

$$v_{WLM,i} = \frac{87,600 \times (m_{(i-1)} - m_i)}{S \rho t_i} \quad (1)$$

where  $m_i$  and  $m_{(i-1)}$  are the coupon weights of the sampling  $i$  and  $(i - 1)$  in g, respectively;  $S$  represents the exposed surface area in  $\text{cm}^2$ ;  $\rho$  is the steel density in  $\text{g}/\text{cm}^3$  and  $t_i$  is the interval corrosion time between sampling  $i$  and  $(i - 1)$  in h.

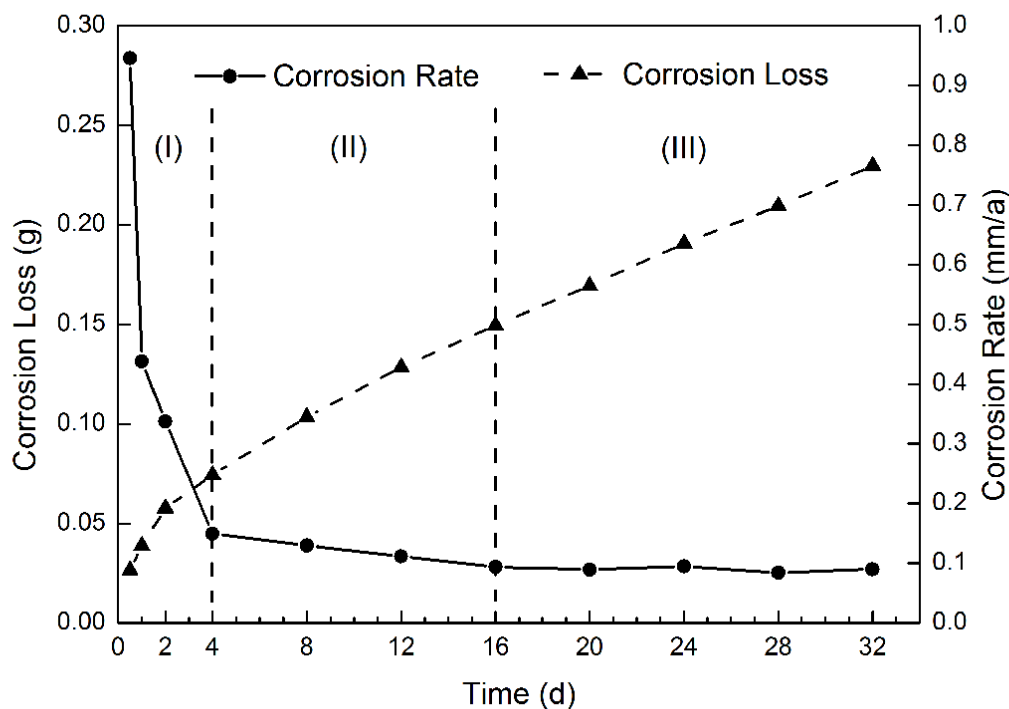


**Figure 5.** Corrosion loss and rate of DI calculated by WLM.

With the growth of corrosion scale, the corrosion rate can be divided into three stages. The first stage lasts for four days and the corrosion rate declines sharply from 0.9455 to 0.1492 mm/a. The second stage turns to slowly decrease from 0.1492 to 0.0936 mm/a during days 4~16. In the third stage, after day 16, the corrosion rate maintains at a very low value around 0.0900 mm/a.

### 3.1.3 Corrosion stage

Considering the similar variation characteristics of scale morphologies and corrosion rates, it can be concluded that the scale is a very effective protective layer for DI and the status of scales directly determines the corrosion rate. In the first stage (before day 4), the thin and incomplete scale layer induced a high corrosion rate. The scale grows very quickly and corrosion rate declines sharply during this stage, thus it can be defined as 'initial stage'. In the second stage (day 4~16), the loose and smooth scale covering the entire coupon surface gradually grow and the corrosion rate decreases slowly. Then it can be defined as 'developmental stage'. In the third stage (after day 16), the scale was compact enough to prevent DI coupons from further corrosion. But under the flushing effect of water, a tiny portion of scales was occasionally flushed away. Then the localized corrosion occurred on the damaged scale surface, eventually leading to the formation of tubercles. Compared with the first two stages, the scales grow slowly and the corrosion rate remains at low value in the third stage, so it can be defined as 'stable stage'.

### 3.2 Electrochemical measurement analysis

#### 3.2.1 Corrosion tendency variation

OCP changed with the growth of corrosion scales, and it can reflect the corrosion tendency of DI. Before each EIS measurement, the steady-state OCP is recorded and its variation curve is shown on Figure 6.

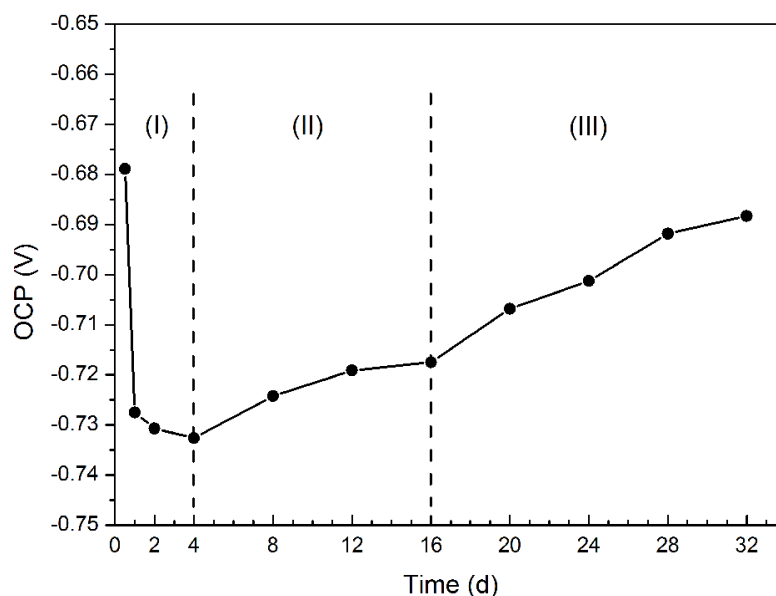


**Figure 6.** OCP variation of DI in simulated WDS.

As can be seen on Figure 6, the variation of OCP also can be divided into three stages. It declined quickly from -0.6789 to -0.7326 V in the initial stage (12h~4d) and then turns to a rising stage both in the developmental (4d~16d) and stable (16d~32d) stages. But the OCP increasing rates of the stable stage ( $1.824 \times 10^{-3}$  V/d) is slightly higher than the developmental stage ( $1.260 \times 10^{-3}$  V/d). It indicates that the compact corrosion scale of the stable stage effectively reduce the corrosion tendency of DI.

#### 3.2.2 Scale structure characteristics

Nyquist impedance plots of DI are shown on Figure 7. With the growth of corrosion scales, three types of Nyquist plots appears. Before day 2 [Figure 7 (a)], it shows a high-frequency tail and a low-frequency capacitive loop. On days 2, 4, 8 and 12 [Figure 7 (b)], it shows a high-frequency tail, a middle-frequency capacitive loop and a low-frequency capacitive loop. On days 16, 20, 24 and 32 [Figure 7 (c)], the low-frequency capacitive loop turns to be a finite layer diffusion impedance. The high-frequency tail is typically related to the surface film of insoluble corrosion products [16, 21] that corresponds to the outside layer of the scales. The middle-frequency capacitive loop is associated with the inside layer of the scales and the low-frequency capacitive loop with the electrical double layer.

The finite layer diffusion impedance appears after the formation of adequately protective scales. Thus, in initial stage (before day 4), the outside layer and inside layer successively formed and covered the entire surface. In developmental stage (day 4 to 16), the two layers of scales gradually developed in thickness and density. In stable stage (from day 16 to day 32), the double-layer scales was compact enough for finite layer diffusion impedance to be generated.

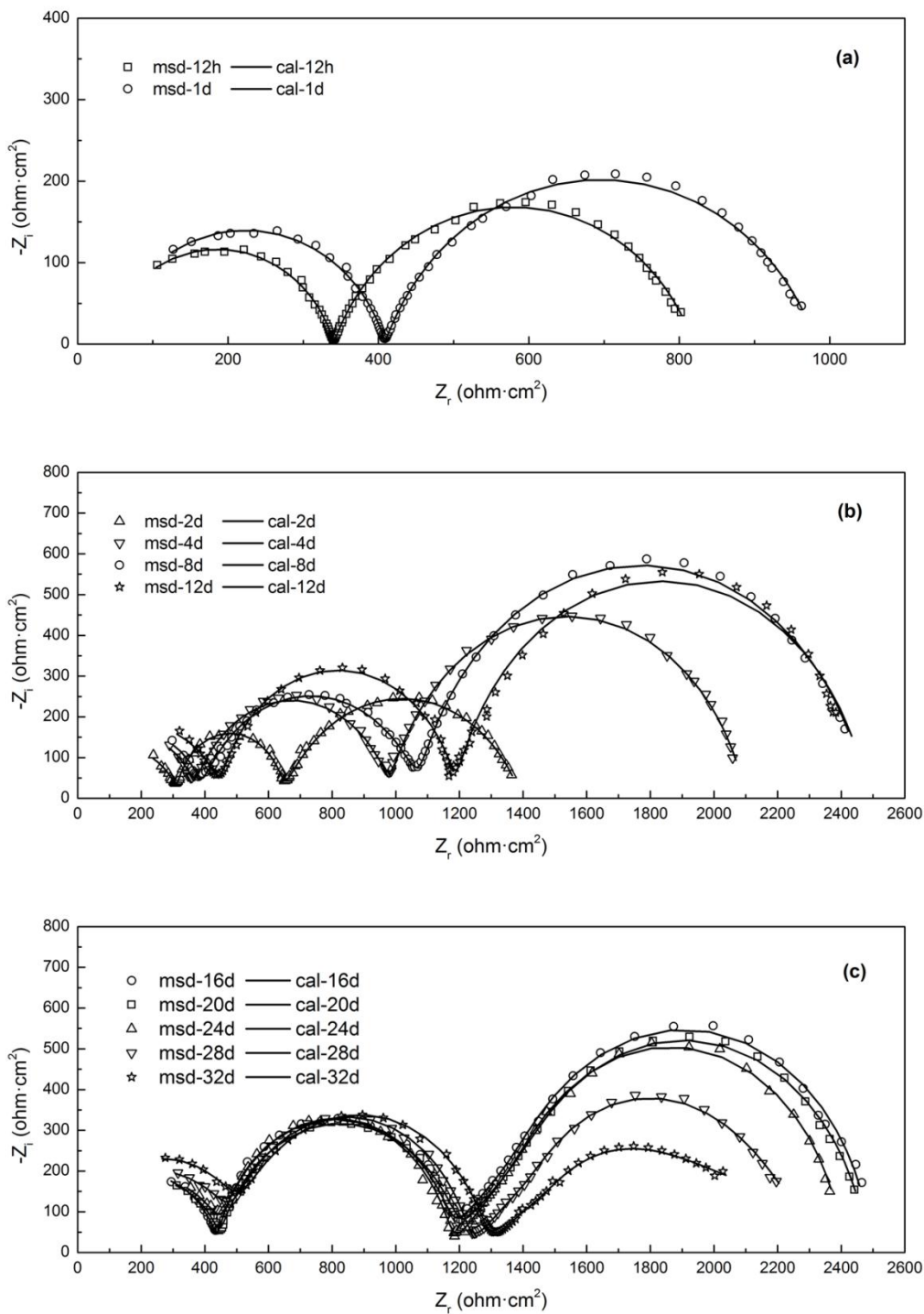
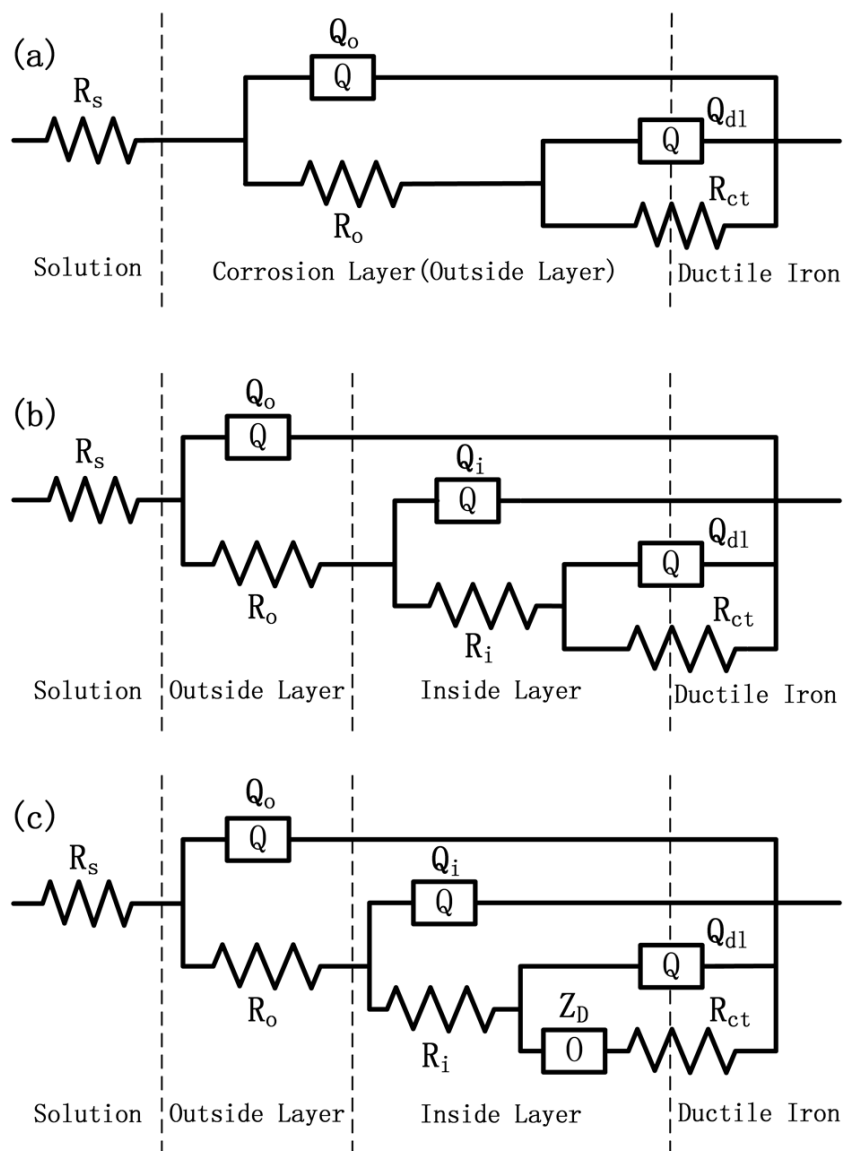


Figure 7. EIS plots of DI in simulated WDS.

3.2.3 Scale physical models



**Figure 8.** Physical models and equivalent circuits applied to fit the EIS plots of DI.

To accommodate for the three structures of corrosion scales, different equivalent circuits should be used to fit the EIS plots. An equivalent circuit proposed by L. Bousselmi [22] is used for reference. Although this equivalent circuit is well suited for carbon steel, some necessary modifications are implemented with the equivalent circuit to account for the different characteristic corrosion scales of DI and carbon steel. To address the inhomogeneities of the corrosion scale of DI, a constant-phase element (CPE) capacitor is a better choice for examining the capacitive behaviour than the capacitors in the equivalent circuit. The pseudocapacitance associated with the CPE ( $C_Q$ ,  $F/cm^2$ ) is calculated by Equation (2) [23]:

$$C_Q = \frac{(Y_0 R)^{1/n}}{R} \tag{2}$$

where parameter  $Y_0$  is in  $S \cdot sec^n / cm^2$ ,  $R$  is the electrical resistance in parallel with the CPE in  $ohm \cdot cm^2$ , and  $n$  is the CPE power.

The schematic of the physical models of DI scales and its corresponding equivalent circuits are illustrated on Figure 8.  $R_s$  represents the solution resistance,  $Q_o$  and  $Q_i$  are the constant phase element related to the outside and inside layer of the scale, respectively, and  $R_o$  and  $R_i$  are the resistance of the outside and inside layer.  $Q_{dl}$  is the constant phase element related to the electronic double-layer capacitance,  $R_{ct}$  is the charge-transfer resistance, and  $Z_D$  is the finite layer diffusion impedance. The finite layer diffusion impedance is described by Equation (3):

$$Z_D = \frac{\tanh(B\sqrt{j\omega})}{Y_0\sqrt{j\omega}} \tag{3}$$

where  $B = l/\sqrt{D}$ ,  $l$  is the stagnant (Nernst diffusion) layer thickness,  $D$  is the diffusion coefficient, and  $Y_0$  is the finite length diffusion element containing the diffusion coefficient.

### 3.2.4 Scale structure transformation

Equivalent circuit (a) is used to fit the EIS plots for hour 12 and day 1, (b) is used for days 2, 4, 8 and 12, and (c) is used for days 16, 20, 24, 28 and 32. The results are displayed on Figure 7 and fit the measured data very well. The fitted parameter values are shown on Figure 9 and used to analysis the scale structure transformation.

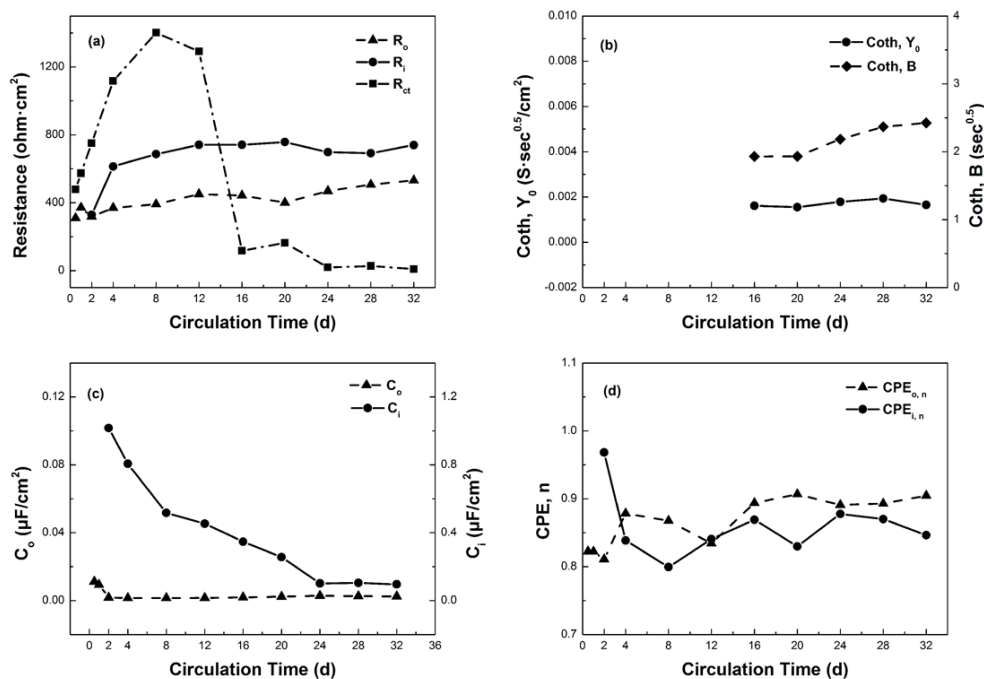


Figure 9. EIS parameters of DI obtained by fitting with the equivalent circuits plotted in Figure 8.

Figure 9 (a) displays  $R_o$ ,  $R_i$  and  $R_{ct}$  variations for different days.  $R_{ct}$  is obviously higher than  $R_o$  and  $R_i$  before day 16, thereafter  $R_{ct}$  quickly declines lower than  $R_o$  and  $R_i$ . It means that the charge transfer primarily controls the corrosion rate in the initial and developmental stages. In stable stage, the finite layer diffusion impedance appears, meaning the mass diffusion turn to the control step of corrosion rate. Figure 9 (b) shows the variations of diffusion branch parameters in stable stage. Parameter  $Y_0$  remains at a low value of approximately  $1.700\text{E-}03 \text{ S}\cdot\text{sec}^{0.5}/\text{cm}^2$ . This indicates the diffusion coefficient essentially remains almost unchanged. Whereas parameter  $B$  shows an obvious increase (from 1.930 to  $2.425 \text{ sec}^{0.5}$ ) during this period, indicating increasing diffusion layer thickness (the thickness of the corrosion scale). This could be caused by the variation of inner film thickness as a result of the continuous deposition-dissolution process on the metal surface under water flow[17].

On Figure 9 (c), the outside layer's pseudo-capacitance value ( $C_o$ ) keeps at a lower constant value (with an average of  $1.836\text{E-}03 \mu\text{F}/\text{cm}^2$ ) than the inside layer's pseudo-capacitance value ( $C_i$ ) during the entire experiment. This indicates that the outside layer is an effective protective layer against corrosion than inside layer, which is consistent with P. Sarin et al. [2]. While  $C_i$  declines with the growth of corrosion scales and finally drops a relatively low value ( $1.636\text{E-}01 \mu\text{F}/\text{cm}^2$ ), suggesting the inside layer also turns to be more and more protective.

Figure 9 (d) shows the CEP power of the outside layer ( $CPE_{o,n}$ ) fluctuates before day 16 and thereafter settles at about 0.9, suggesting the outside layer is unstable in the first two stages and becomes compact in stable stage. While the CEP power of the inside layer ( $CPE_{i,n}$ ) declines in initial stage and then fluctuates around 8.5 in developmental and stable stages. This suggests that a thin and compact inside layer firstly forms and then gradually grows to be porous.

In conclusion, corrosion scales play an important role on DI corrosion control. In the first two stages, charge transfer is restricted by the metal-scale interface. Entering the final stage, scales become compact enough to control the mass diffusion of cathodic depolarizing substances (oxygen). Thereinto, the outside layer of scales is more protective than the inside layer all the time, and both of them become relatively stable in the final stage.

### 3.3 Scales physicochemical characteristics

The scales were viewed in SEM images to visualize their formation. The typical micrographs are shown on Figure 10. The chemical composition and crystalline phase of the corrosion scales were characterized using EDS (listed in Table 3) and XRD (on Figure 11). The physicochemical characteristics of scales change slowly, so typical results of three stages are selected to be discussed. Day 2 is used to study the characteristics for initial stage, day 4 and 8 are used for developmental stage, and day 16 and 32 are used for stable stage. In the first sixteen days, inside and outside layers of the scales cannot be well separated, so these four samples are mixed corrosion products of the two layers. On day 32, the outside layer is compact and thick enough to be stripped off, and the characteristics of inside and outside layers can be studied respectively.

Figure 10 depicts the SEM images of the scales. In initial stage (2d), needle-like and amorphous corrosion products were mainly generated, indicating iron oxides has low degree of

oxidation. In developmental stage, block-shaped and cauliflower-shaped minerals (4d) gradually grow into spherical and block-shaped crystals (8d) with the gradual increasing of crystalline size. Entering stable stage (16d and 32d), spherical and block-shaped crystals became the primary components of the scales, and the maximum diameter of crystals can achieve nearly  $1.5\ \mu\text{m}$  much larger than that of the first two stages. Comparing the two layers of the scales, the inside layer (32d-Inside) is more porous than the outside layer (32d-Outside), which is consistent with the results of EIS analysis.

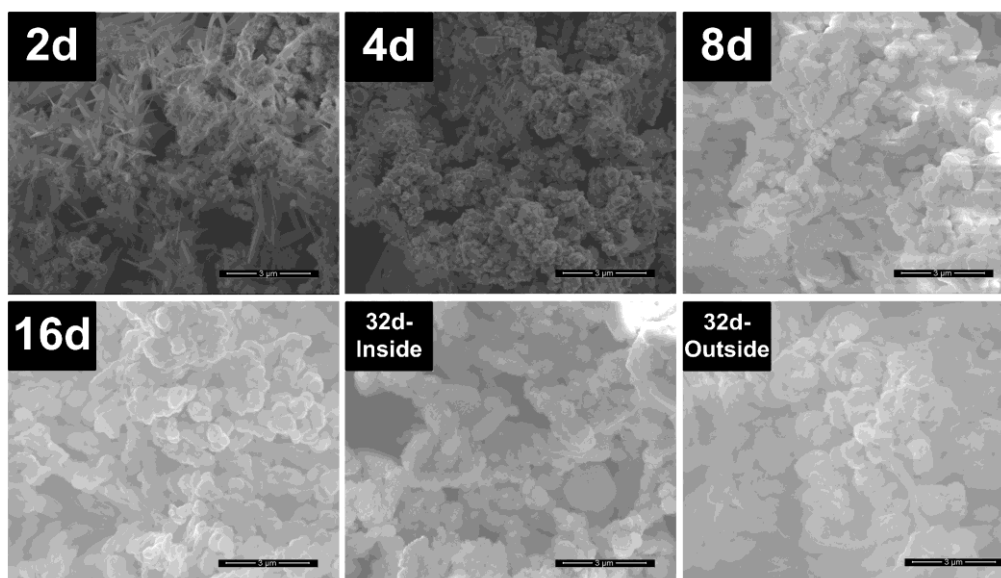


**Figure 10.** SEM images of corrosion scales of DI.

As shown in Table 3, the major components of the corrosion scales are iron (Fe) and oxygen (O), with the total percentage of 85.25~91.45%. This indicates that iron oxides were the primary corrosion products. The presence of carbon (C) and silicon (Si) indicates that both components were possibly released from the metal substrate. It should be noted that calcium (Ca) appeared in stable stage (day 16 and 32), which may come from the tap water used for this experiment.

**Table 3.** EDS analysis of elemental composition of corrosion scales samples<sup>[a]</sup>.

Sample	C	O	Si	Ca	Fe
2d	13.58	45.24	1.17	-	40.01
4d	8.30	42.28	0.59	-	48.84
8d	9.23	47.72	0.82	-	42.23
16d	7.24	48.47	0.86	0.45	42.98
32d-Inside	8.00	45.04	1.78	0.68	44.50
32d-Outside	7.01	46.31	1.53	1.89	43.26

<sup>[a]</sup>All values are in atom% with an error of  $\pm 5\%$

Combining EDS with XRD analysis of the scales (shown on Figure 11), it can be concluded goethite ( $\alpha$ -FeOOH), lepidocrocite ( $\gamma$ -FeOOH), and magnetite ( $\text{Fe}_3\text{O}_4$ ) are the three predominant iron minerals in the scales, which is consistent with existing literature [2, 4]. Before day 16, the content of siderite ( $\text{FeCO}_3$ ), as a stable ferrous solid [24], decreased with corrosion time, indicating  $\text{FeCO}_3$  was further oxidized to ferric phases. On day 32,  $\text{FeCO}_3$  was present only in the inside layer of the scales, suggesting that ferrous oxides mainly exist in the lower part of scales. Both of the results demonstrated that Fe(II) phases were the direct oxides of iron and then oxidized to Fe(III) phases. With the increasing days,  $\text{Fe}_3\text{O}_4$  diffraction intensity of peaks is significantly reduced, while the intensity of  $\alpha$ -FeOOH is increased. It indicates that  $\alpha$ -FeOOH is a more stable component of the scales than  $\text{Fe}_3\text{O}_4$ . Entering stable stage (16d and 32d), calcite ( $\text{CaCO}_3$ ) began to appear in the scales. This is consistent with the EDS analysis and the presence of  $\text{CaCO}_3$  makes the scales become a protective film. On day 32, the  $\text{CaCO}_3$  content of outside layer is higher than inside layer. It can be speculated that  $\text{CaCO}_3$  mainly deposits on the surface of scales and only a portion of  $\text{CaCO}_3$  can penetrate into the inside layer of scales, which again demonstrates the outside layer is more effective in corrosion resistance than the inside layer.

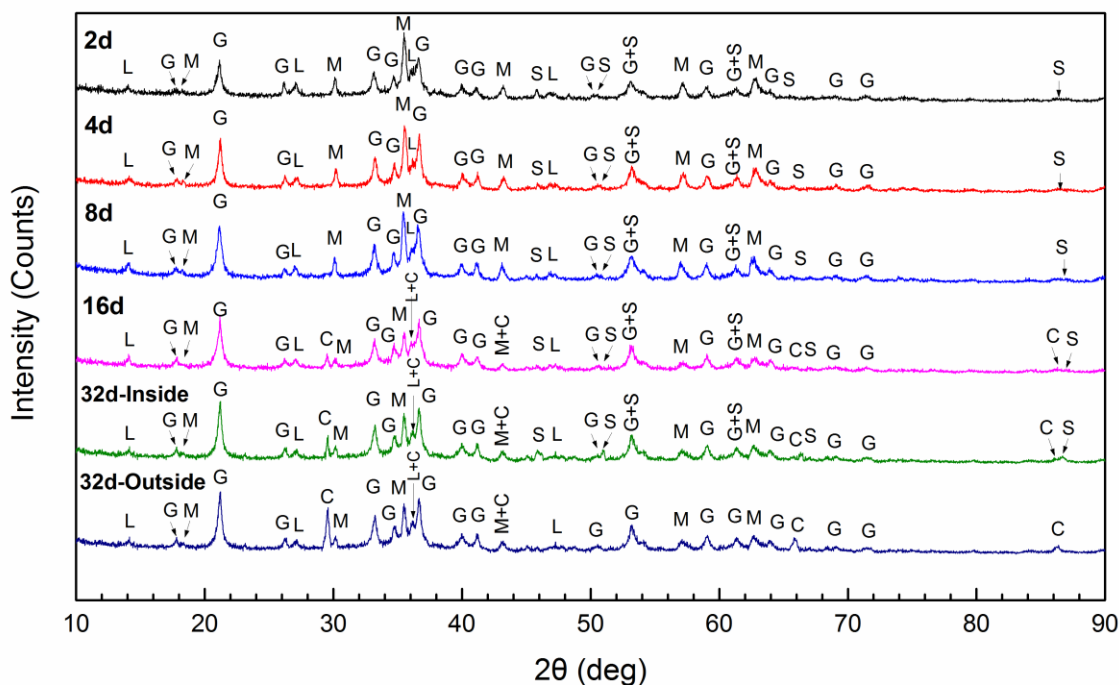


Figure 11. XRD patterns of corrosion scales of DI.

### 3.4 New insights on growth of corrosion scales

Based on the above analysis, the mechanism of scale growth and related corrosion reactions can be presented as the following three stages: the formation process of scales in initial stage, the uniform growth of scales in developmental stage, and the formation and growth of tubercles in final stage.

In initial stage, a single layer of thin and loose scales uniformly forms on the clean iron pipe surface caused by iron oxidation. Because the tap water is with neutral pH (7.13) and high DO concentration ( $6.27 \text{ mg}\cdot\text{L}^{-1}$ ). Thus dissolved oxygen (DO) is the predominant electron acceptor participating in the cathodic reaction. The ferrous ions ( $\text{Fe}^{2+}$ ) produced by the anodic reaction firstly deposit as Fe(II) solids on the corroding metal surface, and then are oxidized to Fe(II)-Fe(III) phases ( $\text{Fe}_3\text{O}_4$ ) and Fe(III) phases ( $\alpha\text{-FeOOH}$  and  $\gamma\text{-FeOOH}$ ). DO diffuses from the bulk water to the corroded floor. So the portion of the scales closet to the scale-water interface is expected to have higher amounts of iron in the ferric state, while the region closest to the metal-scale interface have more ferrous phases. With the continues corrosion, the single-layer scales grow to double-layer scales. During this time, the increasing compactness of outside layer makes less oxygen diffuse to the metal-scale interface, resulting in the decline of corrosion rate. But a portion of the loose scales are easy to be washed away by hydraulic scouring action of flowing water. Then large amount of DO diffuse from bulk water to the bare metal surface accelerating the corrosion reaction. At an instant, the defects will be filled with regenerated scales. The fast growth of scales cannot stop until a complete coverage on the metal surface in the end of the initial stage.

In developmental stage, the compact outside layer decreases the flux of DO diffusing to the metal-scale interface. While the magnetite content inside the scales has high electronic conductivity and facilitates the movement of electrons outward from the metal-scale interface. Thus, besides the metal-scale interface, the cathodic site may be located at the scale-water interface, or inside the scales. With the continuous scales growth in developmental stage, the increasing thickness and compactness of scales slow the rate of DO diffusion from the bulk water towards the metal-scale interface, resulting in cathodic reaction occurring at the upper part of scales. The further oxidation of magnetite to Fe(III) phases inside the scales reduces the electronic conductivity of the scales and lower the corrosion rate. Then mass diffusion starts to replace charge transfer as the control stop of corrosion rate.

On the whole, general corrosion predominates scale growth in initial and developmental stages. Entering the stable stage,  $\text{CaCO}_3$  precipitates locally on the outer surface of scales, providing perfect resistance to DO transport. Beneath the protective scales without DO transport, the Fe(III) phases can serve as the oxidant to accept electrons. While portions of outside layer scales can randomly be washed away due to the hydraulic scouring action of flowing water. Then DO penetrates into scales primarily through the surface defects under which increasing DO concentration accelerates corrosion reactions. Thus localized corrosion takes place and an tubercle begins to grow. With the oxidation of DO and the precipitation of  $\text{CaCO}_3$ , a new protective layer forms on the tubercle surface and the tubercle stops growing. But this is not the end state. Influenced by water quality change, hydraulic scouring action of flowing water and seasonal fluctuation in temperature, crevices will again appear on the scale surface resulting in the formation of new tubercles. That is the cause of the formation of rough and irregular scales in stable stage.

#### 4. CONCLUSIONS

A simulated WDS with a water quality renewal system was designed to provide a corrosion environment close to the hydraulic and water-quality conditions of the actual WDS. The combination

of coupon test units and electrochemical measurement cell was used to study the growth and characteristics of the corrosion scales of DI.

According to the variation characteristics of corrosion morphology and rate obtained by coupon tests, the corrosion process was divided into three stages: (1) initial stage (before day 4), the thin and incomplete scale grows very quickly and the high corrosion rate declines sharply; (2) developmental stage (day 4~16), the loose and smooth scale covering the entire coupon surface gradually grow and the corrosion rate decreases slowly. (3) stable stage (after day 16), the scales are compact enough to prevent DI coupons from general corrosion and tubercles form caused by the localized corrosion, resulting in the corrosion rate remaining at low value.

Nyquist plots displayed the growth of the scales and different equivalent circuits were established to fit EIS parameters in the corresponding stage. Results showed that the stable scales with a compact outside layer and porous inside layer finally formed on the surface of DI. Prior to the formation of stable scales, the charge transfer acted as the corrosion rate controlling step. Afterwards, mass diffusion turned to be the rate-determining step of the corrosion rate.

Scale physicochemical characteristic analysis illustrated that  $\alpha$ -FeOOH,  $\gamma$ -FeOOH and Fe<sub>3</sub>O<sub>4</sub> were predominant iron minerals of all the three corrosion stages. FeCO<sub>3</sub> were the direct oxides of iron and then oxidized to Fe(III) phases. And  $\alpha$ -FeOOH and CaCO<sub>3</sub> were the stable component of the scales.

According to the coupon tests and EIS measurements, the growth of scales are proposed and displayed in three stages: the formation of scales in initial stage, the uniform growth of scales in developmental stage, and the formation and growth of tubercles in stable stage. According to the scale growth process and its related corrosion reactions, it can be concluded that maintaining the scales, especially the outside layer, in a stable state favors the decrease of corrosion rate and iron release of iron pipes.

#### ACKNOWLEDGEMENT

We are grateful for the support provided by the National Natural Science Foundation of China (No. 51278333) and the Specialized Research Fund for the Doctoral Program of Higher Education of China (20130032110032).

#### References

1. Y. Kleiner, B. Rajani, D. Krys, *J. Infrastruct. Syst.* 19 (2013) 108-119.
2. P. Sarin, V. L. Snoeyink, J. Bebee, W. M. Kriven, J. A. Clement, *Water Res.* 35 (2001) 2961-2969.
3. Z. Tang, S. Hong, W. Xiao, J. Taylor, *Corros. Sci.* 48 (2006) 322-342.
4. T. L. Gerke, J. B. Maynard, M. R. Schock, D. L. Lytle, *Corros. Sci.* 50 (2008) 2030-2039.
5. C. Y. Peng, G. V. Korshin, R. L. Valentine, A. S. Hill, M. J. Friendman, S. H. Reiber, *Water Res.* 44 (2010) 4570-4580.
6. F. Yang, B. Shi, J. Gu, D. Wang, M. Yang, *Water Res.* 46 (2012) 5423-5433.
7. P. Sarin, V. Snoeyink, D. A. Lytle, W. M. Kriven, *J. Environ. Eng.* 130 (2004) 364-373.
8. F. Teng, Y. T. Guan, W. P. Zhu, *Corros. Sci.* 50 (2008) 2816-2823.
9. Y. Zhu, H. Wang, X. Li, C. Hu, M. Yang, J. Qu, *Water Res.* 60 (2014) 174-181.
10. H. Wang, C. Hu, L. Zhang, X. Li, Y. Zhu, M. Yang, *Water Res.* 65 (2014) 362-370.
11. Y. Zou, J. Wang, Y. Y. Zheng, *Corros. Sci.* 53 (2011) 208-216.
12. R. de Levie, *Adv. Electrochem. Electrochem. Eng.* 6 (1967) 329-397.

13. I. Frateur, C. Deslouis, M. E. Orazem, B. Tribollet, *Electrochimica acta* 44 (1999) 4345-4356.
14. O. E. Barciaa, E. D'Eliaa, I. Frateurb, O. R. Mattos, N. Pébère, B. Tribollet, *Electrochimica acta* 47 (2002) 2109-2116.
15. M. Sancy, Y. Goubeyre, E. M. M. Sutter, B. Tribollet, *Corros. Sci.* 52 (2010) 1222-1227.
16. M. Sfaira, A. Srhiri, H. Takenouti, M. Marie de Ficquelmont-Loïzos, A. Ben Bachir, M. Khalakhil, *J. Appl. Electrochem.* 31 (2001) 537-546.
17. J. F. Rios, J. A. Calderón, R. P. Nogueira, *Corrosion* 69 (2013) 875-885.
18. F. Yang, B. Shi, Y. Bai, H. Sun, D. A. Lytle, D. Wang, *Water Res.* 59 (2014) 46-57.
19. X. Li, H. Wang, Y. Zhang, C. Hu, M. Yang, *Int. Biodeter. Biodegr.* 96 (2014) 71-79.
20. X. Li, H. Wang, C. Hu, M. Yang, H. Hu, J. Niu, *Corros. Sci.* 90 (2015) 331-339.
21. S. Dalbinc, G. Maurina, R. P. Nogueiraa, J. Persellob, N. Pommierc, *Surf. Coat. Technol.* 194 (2005) 363-371.
22. L. Bousselmi, C. Fiaud, B. Tribollet, E. Triki, *Electrochimica Acta* 44 (1999) 4357-4363.
23. B. Yeum, Technical note 24 - pseudocapacitance associated with CPE, in: ZSimpWin Programme, EChem Software, 2002.
24. P. C. Singer, W. Stumm, *J. Am. Water Works Assoc.* 62 (1970) 198-202.

© 2016 The Authors. Published by ESG ([www.electrochemsci.org](http://www.electrochemsci.org)). This article is an open access article distributed under the terms and conditions of the Creative Commons Attribution license (<http://creativecommons.org/licenses/by/4.0/>).